Determination of the solid surface energy of tellurium dioxide

G. Guisbiers, E. Badradeen, S. Arscott

Journal of Physics and Chemistry of Solids **193** (2024) 112167

https://doi.org/10.1016/j.jpcs.2024.112167

Determination of the solid surface energy of tellurium dioxide

G. Guisbiers[1,*], E. Badradeen[1], S. Arscott[2]

[1] Department of Physics & Astronomy, University of Arkansas at Little Rock, 2801 South University Avenue, AR 72204, USA

[2] University of Lille, CNRS, Centrale Lille, Univ. Polytechnique Hauts-de-France, UMR 8520-IEMN, F-59000 Lille, France

*Author to whom correspondence should be addressed: gxguisbiers@ualr.edu

ABSTRACT

Tellurium dioxide is an ultra-wide bandgap semiconductor material playing a key role in optoelectronics. However, some of its physico-chemical properties such as the solid surface energy are still unknown. Indeed, the values available in the literature are scarce and contradictory. In this letter, the solid surface energy of tellurium dioxide (paratellurite) has been carefully determined to be 142±7 mJ/m^2. This was achieved by measuring the static contact angles made by various liquids (deionized water, ethylene glycol, mercury and Galinstan®) on top of a tellurium dioxide thin film, in a controlled environment.

Tellurium dioxide (TeO_2) is an important material in optoelectronics [1, 2]. Indeed, it has an ultra-wide energy bandgap [3] ~ 3.3 eV; consequently, transmitting the infra-red part of the electromagnetic spectrum, therefore, it is of great interest for optical waveguides [4]. Furthermore, TeO_2 is also a piezoelectric [5-7] and acousto-optic [8, 9] material. As the current technological tendency is to miniaturize electronic devices, TeO_2 is designed with nanometer scale features [10-14]. To understand surface segregation, surface reconstruction, faceting, adsorption, and growth mechanism of TeO_2 nanostructures, a good knowledge of the surface energy of TeO_2 is required. Such parameter plays an important role at the nanoscale: as the size of the material shrinks to the nanometer size range, the surface-to-volume ratio increases drastically.

Unfortunately, there is no direct methodology to determine experimentally the surface energy of solids. However, the most commonly used indirect methodology to access the surface energy of a solid is to measure static contact angles made by various liquids on the surface of the solid being investigated. This methodology requires the use of Young's equation [15]:

$$\gamma_{sv} = \gamma_{lv}.cos\theta + \gamma_{sl} \quad (1)$$

where γ_{sv} is the solid-vapor surface energy (i.e., the solid surface energy of the material), γ_{lv} is the liquid-vapor surface energy (i.e., the surface energy of the probing liquid), γ_{sl} is the solid-liquid surface energy and θ is the static contact angle defined as the angle between the liquid drop and the solid surface. The solid surface energy of a material is defined as the energy required to create a unit area of new surface by the process of division. By knowing the liquid surface energy of different probing liquids and measuring θ, the difference $\gamma_{sv} - \gamma_{sl}$ can be evaluated. Therefore, the solid surface energy of the material being investigated can be determined by solving the following equation [16]:

$$\frac{d(\gamma_{sv}-\gamma_{sl})}{d\gamma_{lv}} = 0 \quad (2)$$

Indeed, when $\gamma_{lv}cos\theta$ is maximum and positive, the difference between γ_{sv} and γ_{sl} is also maximum and positive; meaning that $d\gamma_{sl}/d\gamma_{lv} = 0$ when $\gamma_{lv} = \gamma_{sv}$. This procedure has already been successfully applied to determine the surface energy of selenium [16].

In order to experimentally determine the solid surface energy of TeO_2, a thin film of tellurium has been deposited on a silicon wafer by e-beam evaporation; then, the film was oxidized in air to obtain a TeO_2 thin film. In this work, the static contact angles, made by the probing liquids on the TeO_2 thin film, have been evaluated in a class ISO 5/7 cleanroom (T=20±0.5°C; RH=45±2%). To avoid any contamination, the thin film surface was cleaned using Very Large Scale Integration (VLSI) grade solvents, then rinsed with de-ionized water and finally dried with nitrogen gas. After this cleaning procedure, the TeO_2 thin film was positioned horizontally onto the sample stage of a commercial contact angle meter (Digidrop, GBX Scientific Ltd, Ireland). The probing liquid was loaded into the syringe equipped with a stainless-steel needle, which released one single droplet by the sessile drop technique onto the thin film surface [17, 18]. A photograph of the droplet on the film was then taken by a high-resolution camera one minute after being deposited [Fig. 1(a)]. Consequently, the static contact angles of the droplets were determined from their profiles by using ImageJ software [19-21] (Table 1). Indeed, both static contact angles (left and right) were measured by aligning a tangent line to the droplet profile at the two three-phase contact points [Fig. 1(a)]. The measurements were repeated three times and a different needle was used with each probing liquid. The volume of each droplet was 5 µl. The diameter of each droplet was less than its capillary length to ensure that the effects of gravity could be ignored. By plotting $\gamma_{lv}.cos\theta$ versus γ_{lv} [Fig. 1(b)], the data can be fitted by a parabolic curve. Indeed, the product $\gamma_{lv}.cos\theta$

increases with γ_{lv} for $\gamma_{lv} < \gamma_{sv}$ whilst the product $\gamma_{lv}.cos\theta$ decreases with γ_{lv} for $\gamma_{lv} > \gamma_{sv}$. Consequently, by differentiating the parabolic curve according Eq. 2, the solid surface energy of TeO_2 was determined around 142±7 mJ/m^2. This value makes sense as it is smaller than the solid surface energy of tellurium, 355 mJ/m^2 [22]. Indeed, the solid surface energy of TeO_2 must be less than the solid surface energy of tellurium as already noted by Saha *et al.* [23] for other oxides [Fig. 1(c)].

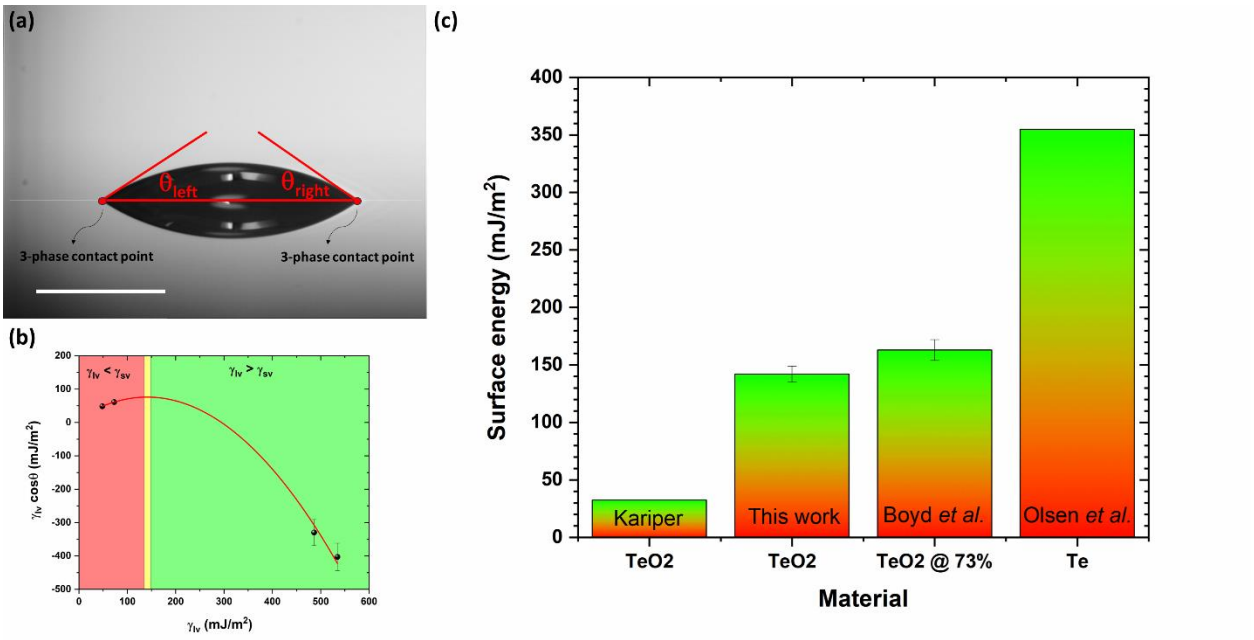

Fig. 1. (a) Photograph showing the static contact angle made by a sessile droplet of DI water on the TeO_2 thin film. The reflection of the droplet on the surface of the film is also visible. These static contact angle measurements were carried out using the sessile drop method. The scale bar represents 1 mm. (b) $\gamma_{lv}\cos\theta$ versus γ_{lv} for a TeO_2 thin film. The red line indicates the evolution of the static contact angle with the liquid surface energy of the probing liquid. Three zones are represented: $\gamma_{lv} < \gamma_{sv}$, $\gamma_{lv} = \gamma_{sv}$, and $\gamma_{lv} > \gamma_{sv}$. The zone where $\gamma_{lv} = \gamma_{sv}$ indicates the possible values

for the solid surface energy of TeO_2. (c) Comparison of the surface energy of various tellurium-based compounds available in the literature.

Table 1. Liquid surface energy of each probing liquid and average static contact angle made by the probing liquid on the TeO_2 thin film.

Probing liquid	**Surface energy, γ_{lv} (mJ/m^2)**	**Static contact angle, θ (°)**
Ethylene glycol	48.4 @ 20°C [24]	2.5 ± 2.5
DI water	72.8 @ 20°C [24]	33.0 ± 0.5
Mercury	486.4 @ 20°C [25]	132.7 ± 6.2
Galinstan®,*	534.6 @ 28°C [26, 27]	138.9 ± 6.7

*Galinstan®, is a liquid alloy of 68.5% Ga, 21.5% In, and 10.0% Sn, which is commercially available from Geratherm® Medical AG in Germany [28].

In 2018, a first attempt to determine the solid surface energy of TeO_2 was performed by Kariper [29] who determined a value around 32 mJ/m^2 by using the Zisman method [30]. The Zisman method determines the critical surface tension of a liquid and assimilates it to the surface energy of the solid when $cos\theta = 1$ which is only true for non-polar surfaces. Unfortunately, TeO_2 is a polar compound as the difference in electronegativity between tellurium and oxygen reaches 1.34. Indeed, to be qualified as non-polar, the difference in electronegativity should not exceed 0.5. Therefore, the value provided by Kariper [29] may not be appropriate to evaluate the solid surface energy of TeO_2. In 2012, another investigation performed by Boyd *et al.* [31] determined the surface energy of a glass made of $73TeO_2$-$20ZnO$-$5Na_2O$-$2La_2O_3$ around 163±9 mJ/m^2. This value

is close to ours but the glass is not made purely of TeO_2 and consequently this value cannot be used either to determine the surface energy of TeO_2 [Fig. 1(c)].

To certify that our thin film surface was only made of TeO_2, the film was characterized by X-ray Photoelectron Spectroscopy (XPS). The acquired spectra revealed the presence of TeO_2 at the surface of the thin film [Fig. 2(a)]. Indeed, it is possible to identify the tellurium oxidation states using the satellite peak features of Te3d. Indeed, the presence of strong satellite peaks around ~ 576 eV and ~586 eV beside the two weak peaks around ~ 573 eV and ~ 583 eV indicates the presence of TeO_2 at the surface of the film. Furthermore, Raman analysis was also performed by using the EZ Raman-I Series from TSI. From the Raman spectra [Fig. 2(b)], the α-phase of TeO_2 (paratellurite) was identified from the peaks sitting at 116 cm^{-1} (E), 136 cm^{-1} (A1) and 264 cm^{-1} (B2).

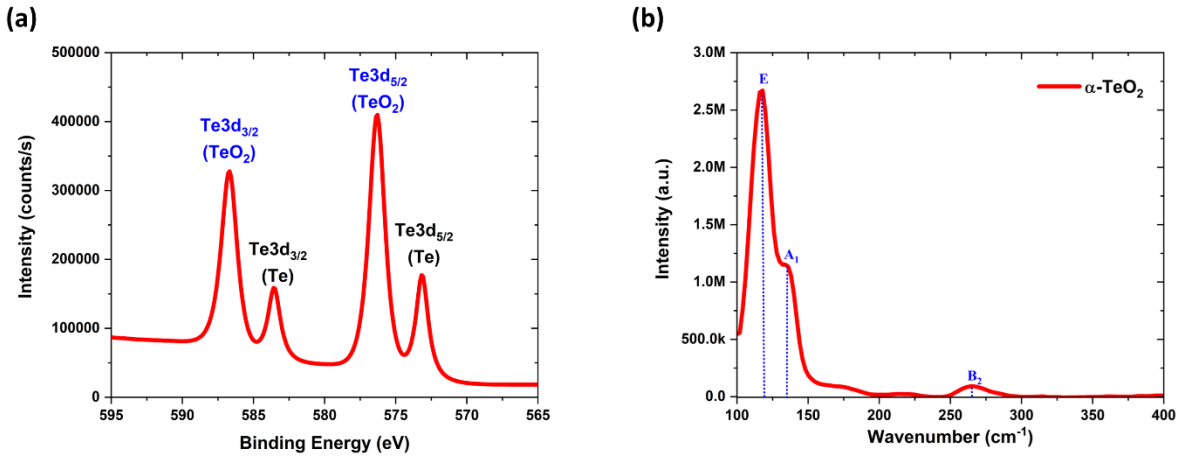

Fig. 2. (a) XPS spectra of the TeO_2 thin film, focusing on the Te3d orbitals. (b) Raman spectra of the paratellurite TeO_2 thin film.

The surface morphology of the TeO_2 thin film has been characterized by scanning electron microscopy and atomic force microscopy. The SEM analysis was performed with a field emission-SEM (JSM7000F from JEOL with energy dispersive X-ray detector, EDX). The AFM analysis was done with a Dimension-Icon AFM from Bruker working in tapping mode at a frequency of 300 kHz. A silicon tip from Ted Pella (Tap300Al-G), exhibiting a tip radius less than 10 nm, a spring constant of 40 N/m and coated with an aluminum layer (~30 nm) on the back of the cantilever to enhance reflectivity, was used as AFM probe. The SEM top-view of the film is shown on Fig. 3(a) while the SEM cross-section view is shown on Fig. 3(b). The thickness of the film is determined to be around 65 ± 3 nm. The AFM image is shown on Fig. 3(c). By analyzing Fig. 3(c) with the WSxM software [32], the RMS roughness was determined to be 4.4 nm. Moreover, the fractal dimension of the thin film was also calculated using the perimeter-area method [33]. Indeed, the surface of an island, A, is linked to its radius R by the relationship $A \sim R^2$. And the perimeter of the island, P, is linked to the fractal dimension of the thin film $D'_{fractal}$with the relation $P \sim R^{D'_{fractal}}$ [34, 35]. When the islands are characterized by a surface with a fractal dimension $D_{fractal}$, the coastlines formed by the islands sectioning by a plane are with a dimension $D'_{fractal} = D_{fractal} - 1$. The relationship linking the perimeter with the surface area is a power law given by $P = \mu A^{\alpha_{fractal}}$ where μ is the proportionality factor between the perimeter and the surface area while $\alpha = D'_{fractal}/2$. The simplest way to obtain $D'_{fractal}$ is to prepare a log–log plot perimeter versus surface area [Fig. 3(d)], where $D'_{fractal}$ can be obtained from the slope α of the linear fit. $D'_{fractal}$ was determined to be around 1.33; consequently $D_{fractal}$ is around 2.33 which correspond to a very smooth surface (i.e. a totally flat surface would have $D_{fractal} = 2$).

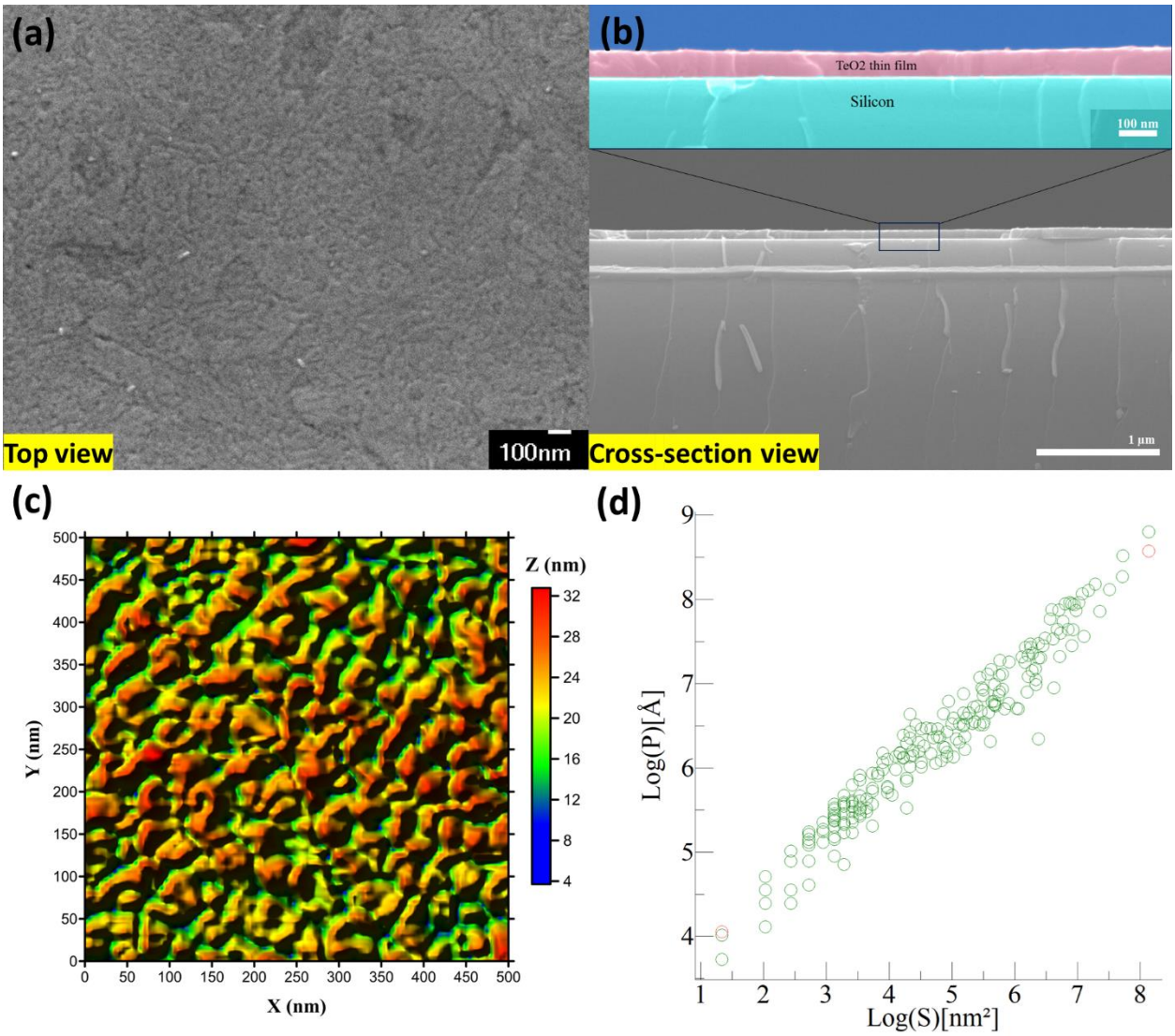

Fig. 3. (a) SEM top view image of the TeO_2 thin film. (b) Cross-Sectional SEM image of the TeO_2 thin film. (c) AFM image of the TeO_2 thin film. (d) Log-log plot of the perimeter versus surface area to determine the fractal dimension of the TeO_2 thin film.

To conclude, four different probing liquids have been used to measure the static contact angles made by those liquids on a paratellurite TeO_2 thin film. The measurements occurred in a cleanroom environment where the temperature and humidity were controlled. Finally, the solid surface energy of α-TeO_2 has been determined experimentally to be 142±7 mJ/m^2.

Acknowledgments

The authors would like to acknowledge Dr. Watanabe from UA Little Rock for his help concerning the acquisition of the XPS spectra.

Authors declarations

Conflict of interest

The authors have no conflict to disclose.

Authors contributions

Gregory Guisbiers: Conceptualization, Project administration, Methodology, Resources, Supervision, Validation, Visualization, Writing/Original draft preparation, Writing/Review and Editing

Emad Badradeen: Data curation, Formal analysis, Investigation, Visualization, Writing/Review and Editing

Steve Arscott: Data curation, Formal analysis, Investigation, Validation, Resources, Writing/Review and editing

Data availability

The data that support the findings of this study are available from the corresponding author upon reasonable request

References

[1] S. Moufok, L. Kadi, B. Amrani, K.D. Khodja, Electronic structure and optical properties of TeO2 polymorphs, Results in Physics, 13 (2019) 102315.
[2] Y. Li, W. Fan, H. Sun, X. Cheng, P. Li, X. Zhao, Structural, electronic, and optical properties of α , β, and γ–TeO2, Journal of Applied Physics, 107 (2010) 093506.
[3] S. Guo, Z. Zhu, X. Hu, W. Zhou, X. Song, S. Zhang, K. Zhang, H. Zeng, Ultrathin tellurium dioxide: emerging direct bandgap semiconductor with high-mobility transport anisotropy, Nanoscale, 10 (2018) 8397-8403.
[4] A. Jha, B.D.O. Richards, G. Jose, T.T. Fernandez, C.J. Hill, J. Lousteau, P. Joshi, Review on structural, thermal, optical and spectroscopic properties of tellurium oxide based glasses for fibre optic and waveguide applications, International Materials Reviews, 57 (2012) 357-382.
[5] V. Rodriguez, M. Couzi, F. Adamietz, M. Dussauze, G. Guery, T. Cardinal, P. Veber, K. Richardson, P. Thomas, Hyper-Raman and Raman scattering in paratellurite TeO_2, Journal of Raman Spectroscopy, 44 (2013) 739-745.
[6] G. Boivin, P. Bélanger, R.J. Zednik, Characterization of Pure Face-Shear Strain in Piezoelectric α-Tellurium Dioxide (α-TeO2), Crystals, 10 (2020) 939.
[7] G. Arlt, H. Schweppe, Paratellurite, a new piezoelectric material, Solid State Communications, 6 (1968) 783-784.
[8] V. Voloshinov, N. Polikarpova, P. Ivanova, K. V., Acousto-optic control of internal acoustic reflection in tellurium dioxide crystal in case of strong elastic energy walkoff, Applied Optics, 57 (2018) C19-C25.
[9] S.N. Mantsevich, M.I. Kupreychik, V.I. Balakshy, Possibilities of wide-angle tellurium dioxide acousto-optic cell application for the optical frequency comb generation, Optics Express, 28 (2020) 13243-13259.
[10] F. Arab, M. Mousavi-Kamazani, M. Salavati-Niasari, Facile sonochemical synthesis of tellurium and tellurium dioxide nanoparticles: Reducing Te(IV) to Te via ultrasonic irradiation in methanol, Ultrasonics Sonochemistry, 37 (2017) 335-343.
[11] G.S. El-Sayyad, F.M. Mosallam, S.S. El-Sayed, A.I. El-Batal, Facile Biosynthesis of Tellurium Dioxide Nanoparticles by Streptomyces cyaneus Melanin Pigment and Gamma Radiation for Repressing Some Aspergillus Pathogens and Bacterial Wound Cultures, Journal of Cluster Science, 31 (2020) 147-159.
[12] G. Guisbiers, L.C. Mimun, R. Mendoza-Cruz, K.L. Nash, Synthesis of tunable tellurium nanoparticles, Semiconductor Science & Technology, 32 (2017) 04LT01.
[13] W.K. Khalef, Preparation and Characterization of Teo2 Nano particles by Pulsed Laser Ablation in Water, Engineering & Technology Journal, 32 (2014) 396-405.
[14] T. Hesabizadeh, E. Hicks, D. Medina-Cruz, S.E. Bourdo, F. Watanabe, M. Bonney, J. Nichols, T.J. Webster, G. Guisbiers, Synthesis of “Naked” TeO2 Nanoparticles for Biomedical Applications, ACS Omega, 7 (2022) 23685-23694.
[15] B.N. Altay, R. Ma, P.D. Fleming, M.J. Joyce, A. Anand, T. Chen, B. Keskin, D. Maddipatla, V.S. Turkani, P.R. Kotkar, A. Fleck, R. Rasheed, D. He, Surface Free Energy Estimation: A New Methodology for Solid Surfaces, Advanced Materials Interfaces, 7 (2020) 1901570.
[16] G. Guisbiers, S. Arscott, R. Snyders, An accurate determination of the surface energy of solid selenium, Applied Physics Letters, 101 (2012) 231606.
[17] M. Ponomar, E. Krasnyuk, D. Butylskii, V. Nikonenko, Y.M. Wang, C.X. Jiang, T.W. Xu, N. Pismenskaya, Sessile Drop Method: Critical Analysis and Optimization for Measuring the Contact Angle of an Ion-Exchange Membrane Surface, Membranes-Basel, 12 (2022).
[18] J. Shang, M. Flury, J.B. Harsh, R.L. Zollars, Comparison of different methods to measure contact angles of soil colloids, Journal of Colloid and Interface Science, 328 (2008) 299-307.

[19] C.A. Schneider, W.S. Rasband, K.W. Eliceiri, NIH Image to ImageJ: 25 years of image analysis, Nat Methods, 9 (2012) 671-675.
[20] A.F. Stalder, G. Kulik, D. Sage, L. Barbieri, P. Hoffmann, A snake-based approach to accurate determination of both contact points and contact angles, Colloids and Surfaces A: Physicochemical and Engineering Aspects, 286 (2006) 92-103.
[21] https://imagej.net/ij/plugins/contact-angle.html.
[22] D.A. Olsen, R.W. Moravec, A.J. Osteraas, The Critical Surface Tension Values of Group VIA Elements, The Journal of Physical Chemistry, 71 (1967) 4464-4466.
[23] B. Saha, A. Peschot, B. Osoba, C. Ko, L. Rubin, T.-J.K. Liu, J. Wu, Reducing adhesion energy of micro-relay electrodes by ion beam synthesized oxide nanolayers, APL Materials, (2017) 036103.
[24] N.G. Tsierkezos, I.E. Molinou, Thermodynamic properties of water plus ethylene glycol at 283.15, 293.15, 303.15, and 313.15 K, J Chem Eng Data, 43 (1998) 989-993.
[25] G.H. Perry, N.K. Roberts, Surface-Tension of Mercury between 15-Degrees-C and 50-Degrees-C by the Sessile Drop Method, J Chem Eng Data, 26 (1981) 266-268.
[26] S. Handschuh-Wang, T.S. Gan, M. Rauf, W.F. Yang, F.J. Stadler, X.C. Zhou, The subtle difference between Galinstan (R) and eutectic GaInSn, Materialia, 26 (2022).
[27] T.Y. Liu, P. Sen, C.J.C.J. Kim, Characterization of Nontoxic Liquid-Metal Alloy Galinstan for Applications in Microdevices, J Microelectromech S, 21 (2012) 443-450.
[28] S. Handschuh-Wang, F.J. Stadler, X.C. Zhou, Critical Review on the Physical Properties of Gallium-Based Liquid Metals and Selected Pathways for Their Alteration, J Phys Chem C, 125 (2021) 20113-20142.
[29] I.A. Kariper, Optical properties and surface energy of tellurium oxide thin film, Journal of Optics, 47 (2018) 504-510.
[30] W.A. Zisman, Relation of the Equilibrium Contact Angle to Liquid and Solid Constitution, Advances in Chemistry, 43 (1964) 1-51.
[31] K. Boyd, H. Ebendorff-Heidepriem, T.M. Monro, J. Munch, Surface tension and viscosity measurement of optical glasses using a scanning CO2 laser, Optical Materials Express, 2 (2012) 1101-1110.
[32] I. Horcas, R. Fernández, J.M. Gómez-Rodríguez, J. Colchero, J. Gómez-Herrero, A.M. Baro, WSXM:: A software for scanning probe microscopy and a tool for nanotechnology, Rev Sci Instrum, 78 (2007) 013705.
[33] B. Mandelbrot, How Long Is Coast of Britain - Statistical Self-Similarity and Fractional Dimension, Science, 156 (1967) 636-638.
[34] A.R. Imre, Artificial fractal dimension obtained by using perimeter-area relationship on digitalized images, Appl Math Comput, 173 (2006) 443-449.
[35] G. Guisbiers, O. Van Overschelde, M. Wautelet, P. Leclère, R. Lazzaroni, Fractal dimension, growth mode and residual stress of metal thin films, J Phys D Appl Phys, 40 (2007) 1077-1079.